Experimental analyses of temperature and pressure oscillation frequencies of a flat plate pulsating heat pipe tested under various edge orientation angles and heat loads

Vincent Ayel, Luca Pagliarini, Thibault Van't Veer, Maksym Slobodeniuk, Fabio Bozzoli, Cyril Romestant, Yves Bertin

▶ **To cite this version:**

Vincent Ayel, Luca Pagliarini, Thibault Van't Veer, Maksym Slobodeniuk, Fabio Bozzoli, et al.. Experimental analyses of temperature and pressure oscillation frequencies of a flat plate pulsating heat pipe tested under various edge orientation angles and heat loads. Experimental and Computational Multiphase Flow, 2024, 6 (3), pp.253-264. 10.1007/s42757-023-0178-6 . hal-04699062

HAL Id: hal-04699062
https://hal.science/hal-04699062v1

Submitted on 16 Sep 2024

HAL is a multi-disciplinary open access archive for the deposit and dissemination of scientific research documents, whether they are published or not. The documents may come from teaching and research institutions in France or abroad, or from public or private research centers.

L'archive ouverte pluridisciplinaire **HAL**, est destinée au dépôt et à la diffusion de documents scientifiques de niveau recherche, publiés ou non, émanant des établissements d'enseignement et de recherche français ou étrangers, des laboratoires publics ou privés.

Paper title: Experimental analyses of temperature and pressure oscillation frequencies of a flat plate pulsating heat pipe tested under various edge orientation angles and heat loads

V. Ayel[1] ✉, L. Pagliarini[2], T. Van't Veer[1,3], M. Slobodeniuk[1], F. Bozzoli[2], C. Romestant[1], Y. Bertin[1]

1. Pprime Institute CNRS – ENSMA – Université de Poitiers, UPR 3346, Futuroscope-Chasseneuil, 86961, France

2. Department of Engineering and Architecture, University of Parma, Parco Area delle Scienze 181/A I-43124 Parma, Italy

3. Stellantis – Carrières sous Poissy, 78955, France

✉ vincent.ayel@ensma.fr

Abstract

A closed loop flat plate pulsating heat pipe, filled with Opteon^{TM} SF33 (with a filling ratio of 50%), has been experimentally studied in different orientations: 0° (horizontal), 22.5°, 45°, 67.5° and 90° ("edge": vertical with horizontal channels). The results confirm the interest of such configurations, rarely investigated in the literature, on the thermal behavior of the device and on the regularity of the temperatures and pressure signals: if dried-out occurred in horizontal orientation, increase of inclination angle (starting from 22.5°) led to regular oscillatory movement due to help of gravity pressure drop between channels. The thermal performance remains very similar for the device inclination angles from 45° to 90°. Both FFT and wavelet analyzes of the pressure signal and temperatures of the external wall of the device (measured with IR camera) have been done to

characterize the dominant oscillatory frequencies. These orientations led to dominant frequencies, rarely detected in the literature for other classic configurations (with vertical/inclined channels). Both similar internal pressure and temperature signals, showed that the dominant frequency increases with decreasing angle (from edge to horizontal orientation), but also with increasing applied heat power, and finally tends to spread and disappear for the highest heat loads.

Keywords

Flat plate pulsating heat pipe; Edge orientation; Thermal performances; Infrared; FFT frequency analysis; wavelet.

Nomenclature

a	Scale factor
Bo	Bond number (-)
BHM	Bottom Heated Mode
C	Condenser
d	Inter-channel distance (m)
D	Diameter (m)
e	Evaporator
f	Frequency (Hz)
FFT	Fast Fourier Transform
FPPHP	Flat Plate Pulsating Heat Pipe
FR	Feeling Ratio (%)
g	Gravity acceleration (ms^{-2})
IR	Infrared
l	Liquid

P	Pressure (Pa)
Pw	Power spectrum (-)
PSD	Power spectrum density
$\dot{Q}$	Heat power (W)
R_{th}	Thermal resistance (KW^{-1})
t	Time (s)
T	Temperature (°C)
TC	Thermocouple
v	Vapor
W	Wavelet transform
α	Inclination angle (°)
η	Dimensionless time
λ	Thermal conductivity ($Wm^{-1}K^{-1}$)
ρ	Density (kgm^{-3})
σ	Surface tension (Jm^{-2})
τ	Time shift (s)
Ψ	Wavelet shape
ω_0	Characteristic parameter

1 Introduction

A Pulsating Heat Pipe (PHP) can be defined as a single tube (or a channel, if engraved in a metal plate) rolled up multiple times on itself between hot(s) and cold(s) sources. The capillary dimension of its internal diameter generates a distribution of the fluid in the form of trains of vapor bubbles and liquid plugs separated by capillary forces. The volume variations of the vapor bubbles, associated with evaporating and boiling phenomena, will cause an intense movement of the fluid associated with both

sensible (*via* liquid plugs) and latent (*via* the evaporation of thin liquid films deposited by the menisci) heat transfer. Such heat transfer will be all the more intense and effective as the device is subjected to thermal stress, as long as it remains within its operational range. Many parameters influence their operating behavior, as it has already been widely described and, for example, transcribed in the review papers of Ma (2015), Khandekar et al. (2010) and Marengo and Nikolayev (2018). A major difference comes from the way PHPs are designed: they could present either tubular or flat plate shapes. The latter can be defined as a flat plate with engraved/machined single channel forming a serpentine (Khandekar et al., 2009; Ayel et al., 2021). This plate is sealed with a second smooth plate cover to confine the channel, or the device can be obtained by additive/etching manufacturing.

Flat plate pulsating heat pipes (FPPHPs), due to their design (material/thermal continuity between channels), are often subjected to unstable operation and low thermal performances in horizontal inclination: intermittently stopover phenomena or even complete stop of operation due to early dry-out of the evaporator are specifically attributed to a lack of pressure perturbations between channels (Miyazaki and Arikawa, 1999; Kim et al., 2003; Ayel et al., 2014). But, starting from a dried-out configuration, when the fluid starts to flow, the ends of a U-shape liquid column oscillate in opposite directions. If the amplitude of oscillations is sufficient, liquid flow into the evaporator and vapor flow into the condenser occur, completing the circulation cycle. As the heat load increases, oscillations become larger, with the liquid occasionally overflowing into neighboring turns. Because the phases of liquid column oscillations are not independent from one another, they vary continuously and the menisci at each end move in a waveform (Miyazaki and Arikawa, 1999; Kim et al., 2003); due to the spring effect of the vapor bubbles, the fluid motion is sequentially transmitted from one branch to another along the FPPHPs.

This effect can be enhanced when gravity pressure drop is added to the pressure perturbations between channels. It is obtained when the device is oriented vertically, but with horizontal channels in the so-called “edge” -or “side”- orientation (Ayel et al., 2014; Pagnoni et al., 2018; Ayel et al., 2021).

Pressure imbalance in the liquid slugs is occasioned by difference in height at each U-turn, leading to a particularly high gravity pressure head for the last surrounding bend; this can drive a continuous long-term oscillatory motion between all liquid slugs, even for the lowest heat powers applied, without encountering any dry-out at the evaporator. The liquid slugs oscillate in a waveform from bottom to top, through the vapor phase into the evaporator region, as oscillation velocities and amplitudes increase with heat input augmentation. Pagnoni et al. (2018) performed visualizations of liquid menisci oscillating in a FPPHP tested with ethanol in edge orientation. They found an oscillation dominant frequency increasing from 2.5 Hz at 80 W to 4 Hz at 200 W heat load applied, as well as menisci velocities, demonstrating the regularity of heat transfer under such conditions. Chi et al. (2018) performed Fast Fourier Transform (FFT) analysis of a temperature signal recorded in the evaporator zone of a tubular PHP filled with ethanol and tested with different orientations starting from vertical bottom heated mode (BHM): they found a dominant peak frequency around 0-0.1 Hz in BHM, whereas increasing the filling ratio or the inclination angle both reduce the power spectrum density (PSD) distribution. Xu and Zhang (2005) found dominant fluid oscillation frequencies up to 0.35 Hz at low heat loads, and of 0.46 Hz at high heat loads to the evaporator in a PHP made of copper (wall thickness = 0.5 mm) and partially filled with FC-72. The post-processed signals were temperature data acquired by means of thermocouples placed on the outer wall in the overall device.

However, it has to be stressed that some FFT analyzes on outer wall temperature measurements did not highlight any dominant fluid oscillation frequency in the studied PHP devices. Zhao et al. (2011) performed a FFT analysis on outer wall temperature data acquired in the condenser of a copper PHP (wall thickness = 1.53 mm) at 60 Hz through thermocouples with an accuracy of 0.25°C. The results showed no particular dominant frequency; this remark was confirmed by adopting wavelet transforms on the same set of data. Similar absence of dominant frequency was observed in (Monroe et al., 2017) by the FFT analysis on outer wall temperature signals acquired by thermocouples, where a copper PHP having wall thickness of 1.55 mm was investigated. The presented discrepancy between

the provided experimental results raises doubts about the feasibility of estimating quantitative dominant frequencies starting from thermocouples signals, especially when thicker tube walls are considered. Nonetheless, it is unclear whether such inability of detecting dominant frequency patterns is due to the thermal properties of the wall, to the transient properties of the adopted sensors, to the wall-sensors couplings (Pagliarini et al., 2023a) or to the very absence of a dominant frequency specific to thermal-hydraulic transfer.

Frequency analyzes in PHPs have been also conducted by considering local fluid pressure signals. Despite the complexity of direct fluid pressure measurements implementation, fluid pressure measurements are expected to provide a good insight into the inner fluid dynamics of PHPs, since pressure differences between the evaporator and the condenser promoted by non-equilibrium conditions are responsible for fluid motion in such devices. In (Khandekar et al., 2009; Mameli et al., 2014; Takawale et al., 2019), fluid pressure acquisitions referred to one single measurement point in PHPs charged with ethanol were processed by the FFT method, even though dominant fluid oscillation frequencies were only found in Khandekar et al., 2009. In fact, the latter work dealt with the study of a single-loop PHP, where the oscillatory features of the working fluid might have been less complex and more perceivable by single-point acquisitions than in multi-turn devices. Such a remark could suggest that dominant fluid oscillation frequencies may not always be identified in PHPs due to the intrinsic chaoticity of the fluid motion, especially when several branches interact one with each other. Perna et al. (2020) performed wavelet analysis on two pressure signals taken at both ends of a single channel in a multi-turn PHP, showing that this method is well adapted to fluid oscillations assessment. However, the authors did not stress the fact that the achievement of fluid oscillation frequency estimations could be here allowed by two fluid pressure measurement locations rather than by the adoption of the wavelet method as reduction technique. Nonetheless, by employing thermographic acquisitions collected during the same experimental campaign of Perna et al. (2020), Pagliarini et al. (2021) proved that the non-intrusive infrared measurements on the outer wall surface of the tubes led

to results identical to those obtained with previous pressure signals in terms of dominant fluid oscillation frequency. Here, infrared measurements carried out on the overall adiabatic section were processed by means of the wavelet method. The relevance of using non-intrusive IR thermography on a tubular micro-PHP was confirmed by Iwata et al. (2022). A similar method was used for the investigation of the wall-to-fluid heat fluxes along the adiabatic section (Pagliarini et al., 2022) and fluid oscillations and transverse interactions (Pagliarini et al., 2023b) in a metallic flat plate PHP filled with water/20 wt.% ethanol mixture with 50% filling ratio. In the latter, by using the evaluated wall-to-fluid heat flux distributions of the former as inputs for the wavelet analysis, the authors could assess and quantify the fluid oscillation dominant frequencies in every channel of the device, oriented in both horizontal and vertical bottom heated mode (BHM) orientations. They found that, if there were a higher average activity in vertical BHM (confirming better transfer capability than in horizontal orientation), the fluid motion exhibited a stable dominant oscillation frequency between channels when the device was oriented horizontally. This was attributed to the negligible buoyancy effects, and it confirmed the liquid column waveform oscillations in such orientation, as already observed by Miyazaki and Arikawa (1999) and Kim et al. (2003). When compared to thermocouples attached on the outer wall surfaces, the more robust and repeatable insights provided by thermography on the inner fluid dynamics of PHPs seem to confirm that transient characteristics of contact temperature sensors cannot always allow an effective identification of temperature variations during the PHP operation.

At the light of the disagreeing results proposed in the previous literature, it is still not clear whether the reported absence of dominant fluid oscillation frequencies in some studies on PHPs are to be attributed to ineffective post-processing methods, to unsuitable experimental signals (i.e., uncapable of reflecting the inner fluid-dynamics of the system) or to the intrinsic chaoticity of fluid motion in PHPs.

This experimental work aims, on one hand, at filling such literature gap by disclosing the potentialities of different reduction techniques for the fluid oscillation frequency estimation in PHPs,

as well as by investigating the suitability of different experimental signals for the sake of characterizing the fluid oscillatory behavior. A FPPHP filled with OpteonTM SF33 is studied by carrying out thermographic and direct fluid pressure measurements, as well as outer wall temperature measurements by means of thermocouples. The tests are conducted during the device operation under different heat loads to the evaporator and edge inclination angles. In particular, studies on PHPs tested under edge orientation are rather rare in the literature (Ayel et al., 2021), and the impact of such working configuration on fluid oscillations and overall thermal behavior is not yet clearly assessed. The collected experimental data are thus reduced by means of both the FFT and wavelet methods to estimate dominant fluid oscillation frequencies characteristic of the device under investigation, thus disclosing the effects of the edge orientations on the oscillatory behavior. A thermal characterization of the FPPHP is furthermore achieved by evaluating equivalent thermal resistances, thus providing links between the overall thermal performance and fluid oscillations.

2 Experimental apparatus

The FPPHP consists of a copper plate (80x200x3.5 mm^3) machined with a single square shaped groove (3x3 mm^2) forming a series of 8 U-turns in the evaporator (see Fig. 1a). This first plate was covered with a second brazed one (0.5 mm thick). Both were brazed with tin to guarantee perfect sealing. Sealing test and vacuuming were made thanks to a Pfeiffer Vacuum® pump coupled with a helium detector (ASM 142 Adixen). The evaporator zone is heated by a wire electrical heater (Thermocoax®, 1 mm diameter), embedded in a copper plate brazed on the back side of the FPPHP (40x80x2 mm^3), and connected to electrical power supply (ELC® ALR3220, ±10 mV). On the opposite side, the condenser section is cooled by a grooved brazed copper plate (80x80 mm^2) cooled by water flow from a cryothermostat (Huber® CC240 wl).

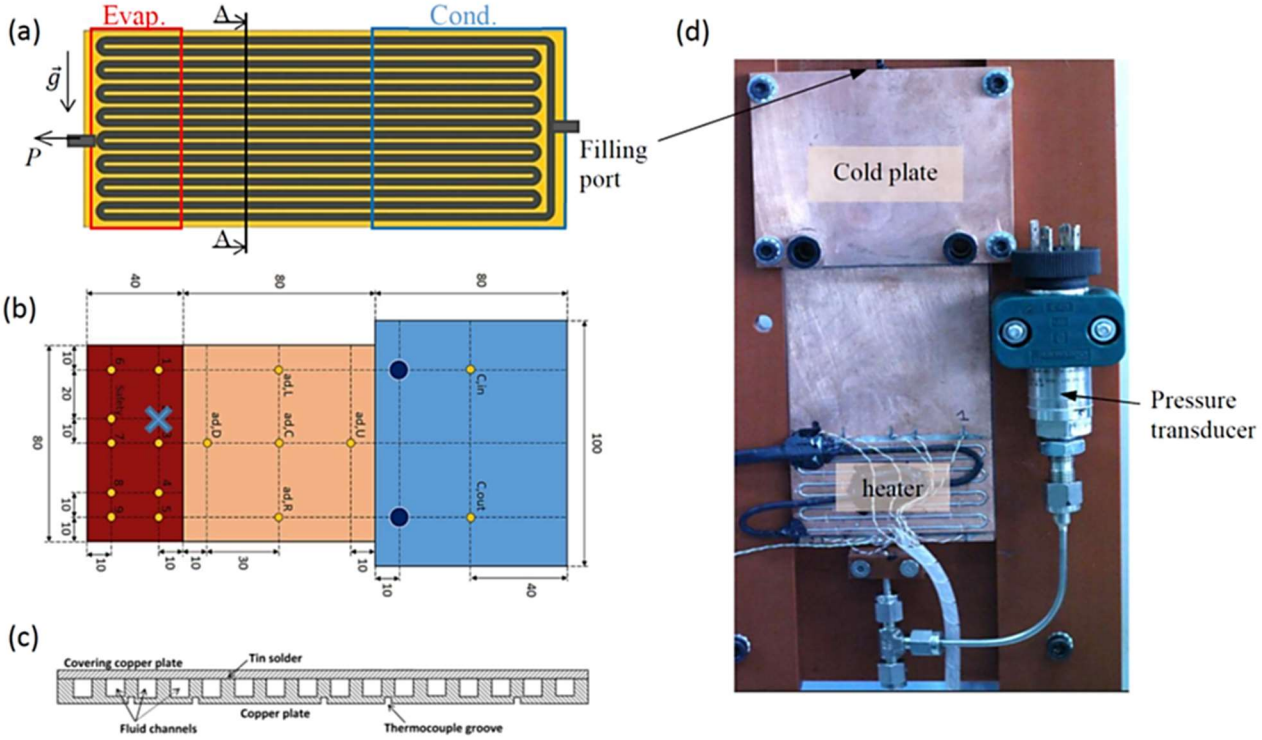

167

168 **Fig. 1** Schematic description of the FPPHP: (a) copper plate with machined grooves (edge orientation);
169 (b) back-side with heater, cold source, and thermocouples positions; (c) A-A cross-section; and (d)
170 photograph of the back-side with heater, cold source and pressure transducer.

171

172 Fifteen T-type thermocouples (TCs, ±0.8 K from internal switch calibration, 0.2 Hz) are used
173 for the temperature measurements between evaporator and heating plate (8 TCs), adiabatic zone (5
174 TCs), and two measure the cold plate temperatures (*C,in* and *C,out*, Fig. 1b). Two connection pipes
175 were brazed on the device (Fig. 1a): one for the filling; the other, in a central bend of the evaporator
176 zone, leading to a tee, connected to a pressure sensor (GE® PTX5076, ±200 Pa, 100 Hz) and a plug
177 for emptying process. Finally, the device top face has been coated with a highly emissive paint
178 (emissivity: 0.95, ±0.1) for infrared visualizations thanks to an infrared camera (INFRATEC®, 10 Hz)
179 in order to detect the impact of internal thermofluidic interactions on the external wall temperature
180 distribution. The camera is always oriented in the direction of the normal to the external black painted

face. All other faces of the FPPHP have been thermally insulated using 50 mm of Rockwool ($\lambda \approx 0.04$ W.m^{-1}K^{-1}).

Before filling, the device was cleaned using Finox® and rinsed several times. In the following, OpteonTM SF33 was chosen as the working fluid (appropriate for replacing HCFCs, HFC, etc.). Based on the widely used critical diameter derived from the Bond number criterion for static conditions ($D_{crit} \approx 2.74\sqrt{\sigma/g(\rho_l - \rho_v)}$ (Drolen and Smoot, 2017)), this gives approximately 3 mm at 20°C and 2.71 mm at 50°C. This means that the channel of the FPPHP can be above D_{crit}, leading to a stratification of the liquid/vapor phases, particularly in vertical orientation. However, such criterion remains hardly quantifiable when considering non-circular channels with sharp angles, such as the ones considered in this study (Ayel et al., 2021).

The operating conditions are summarized below:

- Volumetric filling ratio: FR = 50% at 20° C;
- Cold source: water set at 20° C;
- Heat power applied: 25–50–100–150–200 W;
- Inclination: from horizontal (α = 0°) to vertical edge (α = 90°), with 3 intermediate steps: 22.5°, 45° and 67.5° (Fig. 2).

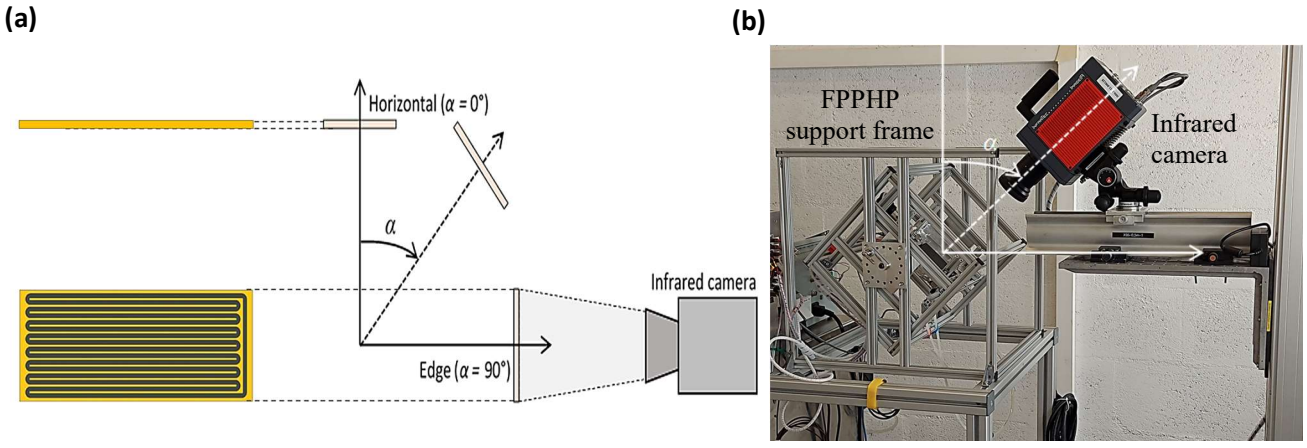

Fig. 2 Experimental set-up: (a) Schematic description and (b) Photograph of the test bench.

Finally, let us mention that the gravity pressure head between two adjacent channels ($\Delta P_g = \Delta P_{g,0} sin(\alpha)$, where $\Delta P_{g,0} = \rho_l g d$, and d the inter-channel distance) can reach, for the edge inclination, values of $\Delta P_{g,0}$ of 64.9 Pa at 20°C, and 61.1 Pa at 50°C, whereas it reaches 973.3 Pa at 20°C, and 916.4 Pa at 50°C, for the last surrounding bend, which is far above the maximum capillary pressure drop of menisci in the transverse section of the grooves ($\Delta P_{c,max} = 2\,\sigma/(D/2)$ = 21.5 Pa and 16.4 Pa at 20°C and 50°C, respectively). This shows that, in this position, even if the device is dried-out in the evaporator zone, an instability driven by the gravity pressure head between channels will help restarting the FPPHP and even make it operational over a larger heat power range than in horizontal orientation.

3 Results and discussions

3.1 Thermal response of the FPPHP

Fig. 3 presents examples of thermocouples transient temperatures evolutions with increasing heat power steps for the FPPHP tested in horizontal (α = 0°, Fig. 3a), intermediate (α = 45°, Fig. 3b), and edge (α = 90°, Fig. 3c) orientations. On the one hand, in horizontal orientation (Fig. 3a), the FPPHP does not activate, and the temperature curves increase smoothly and progressively. This reflects the typical behavior of a full conductive mode, where liquid plugs are accumulated in the condenser zone and the vapor bubbles in the evaporator zone, leading to device inactivity (Miyazaki and Arikawa, 1999; Kim et al., 2003; Ayel et al., 2014). On the other hand, for the two other configurations (Fig. 3b and c), it can be seen that the overall level of temperatures also increases with increasing heat power, but it stabilizes at levels much lower than in horizontal orientation, , and they decrease with the increasing of the tilt angle α. In both configurations, the temperature curves remain relatively stable, particularly at lowest heat powers (25 W and 50 W). This shows that the device operates quite well in such positions, confirming what stated in previous studies (Ayel et al., 2014; Pagnoni et al., 2018). However, it can be observed that the level of temperature fluctuations increases with increasing heat power, being the result of growing thermo-fluidic instabilities in the device, particularly for α = 45°.

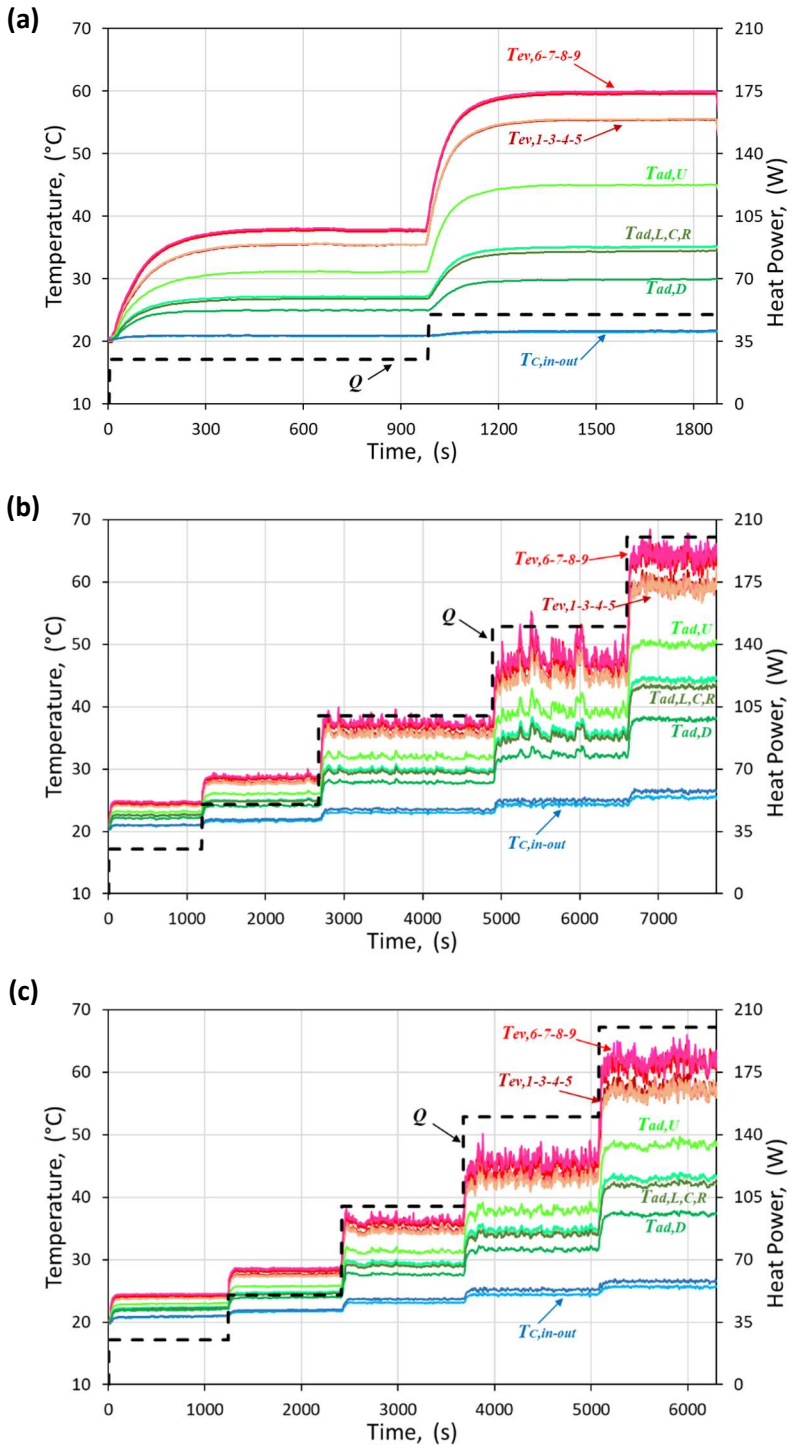

Fig. 3 Transient temperature responses of the FPPHP to increasing heat power levels: (a) α = 0°; (b) α = 45°; (c) α = 90°.

Fig. 4 plots the spatial and temporal average temperature differences $\Delta T_{e\text{-}c}$ between evaporator ($\bar{T}_e = \sum_{i=1}^{8} T_{ev,i}/8$) and cooling fluid ($\bar{T}_c = (T_{c,in} + T_{c,out})/2$)), as well as the thermal resistance obtained in steady-state conditions (averaged over 200 s of consecutive recordings), with their corresponding error bars ($R_{th} = \Delta T_{e-c}/\dot{Q}$, $\dot{Q}$ being the electric power from which the thermal losses have been subtracted, taking into account natural convection and radiation heat transfer from the black coated face). It can be seen that the thermal resistance slightly decreases, as is often the case in literature, for low heat powers from 25 W to 100 W (except for α = 22.5° and horizontal positions, where it increases). However, a slight increase in thermal resistance can be noted from 100 up to 200 W, which is less common in literature. This is probably specific to this modus operandi and remains an open question at this stage of the study. Furthermore, the thermal performances remain very similar for the inclination angles from 90° down to 45°, they slightly decrease for 22.5°, whereas the FPPHP does not activate in horizontal position (0°). For the latter case, the thermal resistance has been, in fact, found equivalent to empty FPPHP operation. It has also to be underlined that there seems to be an inclination angles range (or gravity pressure head) for which the performances (transferred heat and fluid flow) remain independent, here between 90° and 45°. This point requires further investigation.

Note that, in Fig. 4, the error bars correspond to that of measurement error. However, in Fig. 3, the evaporator temperature fluctuation is obvious for some heat powers applied and inclination angles. Such instability level can be quantified using standard deviation from sufficiently long-term samples within the steady-state temperature curves (here, 200 s of steady-state). Standard deviations of the evaporator averaged temperature curves (calculated using the formula: $\sqrt{\{\sum(T_{ev} - \bar{T}_{ev})^2\}/(n-1)}$, with n the number of samples) can consequently be seen in Table 1 for every test cases. This shows that the instability level generally increases with heat power, but apparently regardless of the inclination.

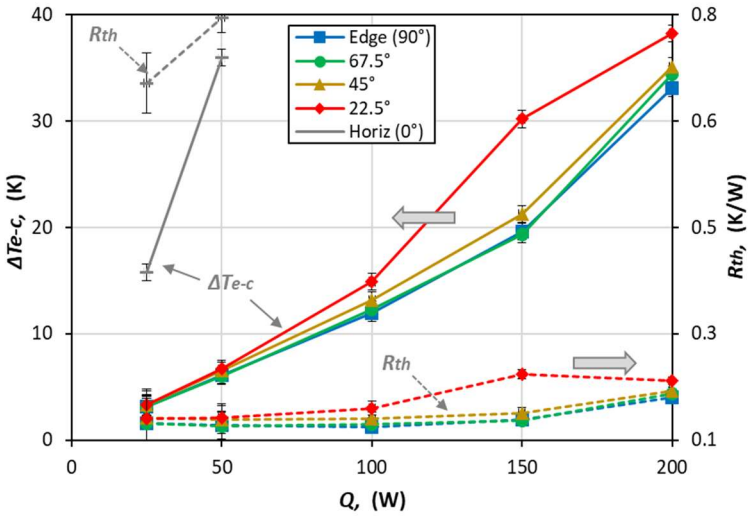

Fig. 4 $\Delta T_{e\text{-}c}$ (-) and R_{th} (--) as functions of heat power applied for the five orientations.

Table 1 Standard deviations of spatial average evaporator temperatures as functions of applied heat power

Inclination angle / Heat power (W)	Edge (90°)	67.5°	45°	22.5°	Horizontal (0°)
25	0.023	0.031	0.038	0.064	0.075
50	0.210	0.069	0.243	0.183	0.030
100	0.712	0.276	0.361	0.717	-
150	1.024	0.819	0.996	0.634	-
200	0.946	0.665	0.734	0.917	-

3.2 Frequency analyzes

As stated in the introduction, the edge orientation was one of the only positions in the literature that made it possible to record a dominant frequency of the overall heat and mass transfer in FPPHPs. First, to understand the best experimental signal and reduction approach to be used for the estimation of fluid oscillation frequencies in the investigated PHP, the thermographic and fluid pressure data were processed by means of both the FFT and the wavelet methods and will be compared in the following section. Then, a systematic frequency analysis based on only FFT method will be done varying the

inclination angle and the heat power applied. The wavelet shape equation chosen for this study is the Morlet wavelet, as defined in the following equation, according to Perna et al. (2020) and Pagliarini et al. (2022-2023b):

$$\psi(\eta) = \frac{1}{\sqrt{\pi}} e^{-\frac{\eta^2}{2}} e^{i\omega_0 \eta} \quad (1)$$

where η is the dimensionless time and ω_0 the characteristic parameter (set at 2π for this study). The wavelet transform (continuous) of a time-dependent signal g thus reads as:

$$W_\psi(a,\tau) = \frac{1}{\sqrt{a}} \int_{-\infty}^{\infty} g(t) \psi^* \left(\frac{t-\tau}{a}\right) dt \quad (2)$$

where the mother wavelet is scaled by the scale factor a and translated by time shifts τ.

(i) ***FFT vs wavelet method: IR camera and fluid pressure signals***

An oscillatory movement can be observed from the successive infrared images of the terminal end of the evaporator in Fig. 5 (here in edge orientation at 150 W heat applied). The U-turns can easily be distinguished from one image to another due to strong evaporative phenomena resulting in a sharp decrease of wall temperature, with an oscillating motion of the working fluid going from bottom to top. It has to be highlighted that, since phase change processes are responsible for pressure increases at the evaporator, they are believed to be inherently linked to the fluid motion towards the condenser, *i.e.*, to the fluid oscillation frequency. Areas used for spectral analysis (4x4 pixels) are delimited by the white squares at the end of each U-turn in the last right-hand side image of Fig. 5. They are numbered from 1 for the upper bend to 8 for the bottom bend. The temperature assigned to each U-turn resulted from a space average of the IR temperatures referred to every pixel belonging to each considered squared area. Such an averaging procedure was needed to reduce the noise level in the thermographic data, while maintaining meaningful information about the physics of the occurring phenomena.

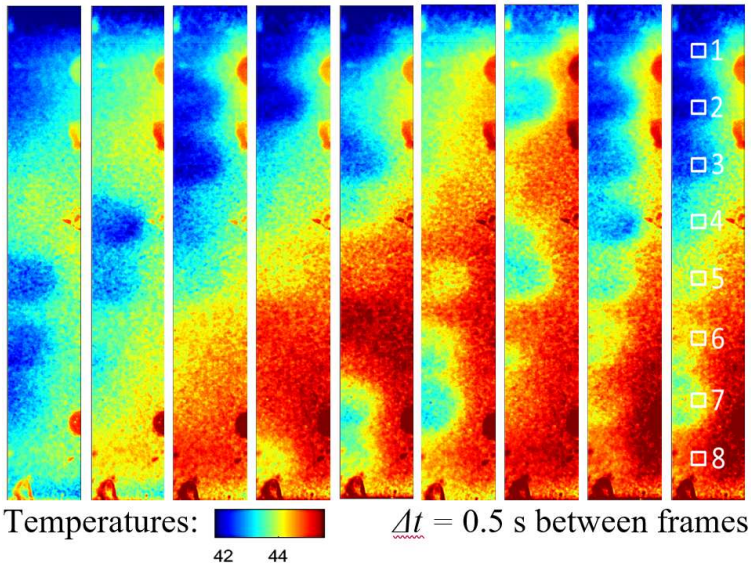

Fig. 5 Infrared visualizations in the evaporator zone (α = 90°; $\dot{Q}$ = 150 W).

In Fig. 6, the average IR signal related to turn 1 in the evaporator and sampled over 60 seconds is shown together with the FFT and wavelet outputs (heat load equal to 50 W, edge orientation). The average temperature signal (Fig. 6a) exhibits strong fluctuations due to phase-change phenomena, which result in significant wall temperature variations. The power spectrum obtained through the FFT method (Fig. 6c) presents a peak at about 0.94 Hz, denoting that the oscillatory behavior is characterized by such a dominant frequency.

Other low-amplitude peaks are here due to either noise in the raw signal or chaotic motion of the working fluid, which oscillates with non-fixed frequency. In Fig. 6b, the time representation of the signal's frequency (magnitude scalogram) provided by the wavelet approach confirms the presence of chaotic fluid oscillations. In fact, despite the signal's power is mainly concentrated at around 1 Hz over the observation window, few time instants present peaks at different frequencies, denoting that the fluid oscillation undergoes sudden variations in terms of oscillation frequency. Nonetheless, the power spectrum obtained through the wavelet method exhibits a peak at 0.94 Hz, i.e., the perceived dominant frequency is the same as that given by the FFT analysis (Fig. 6c). Hence, when IR samples are considered, the frequency analyses carried out by means of different approaches give same results.

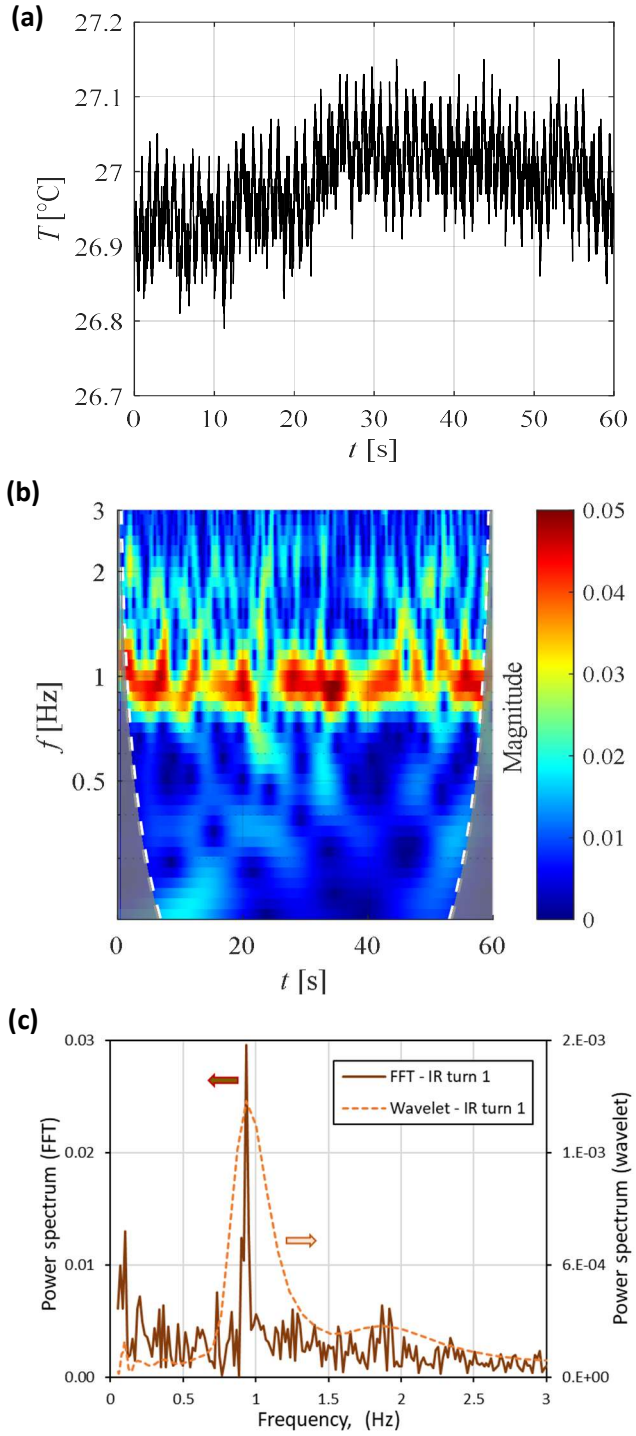

Fig. 6 (a) Space average IR thermographic signal of turn 1 (10 Hz); (b) wavelet magnitude scalogram; (c) power spectra for both FFT and wavelet methods (α = 90°; $\dot{Q}$ = 50 W).

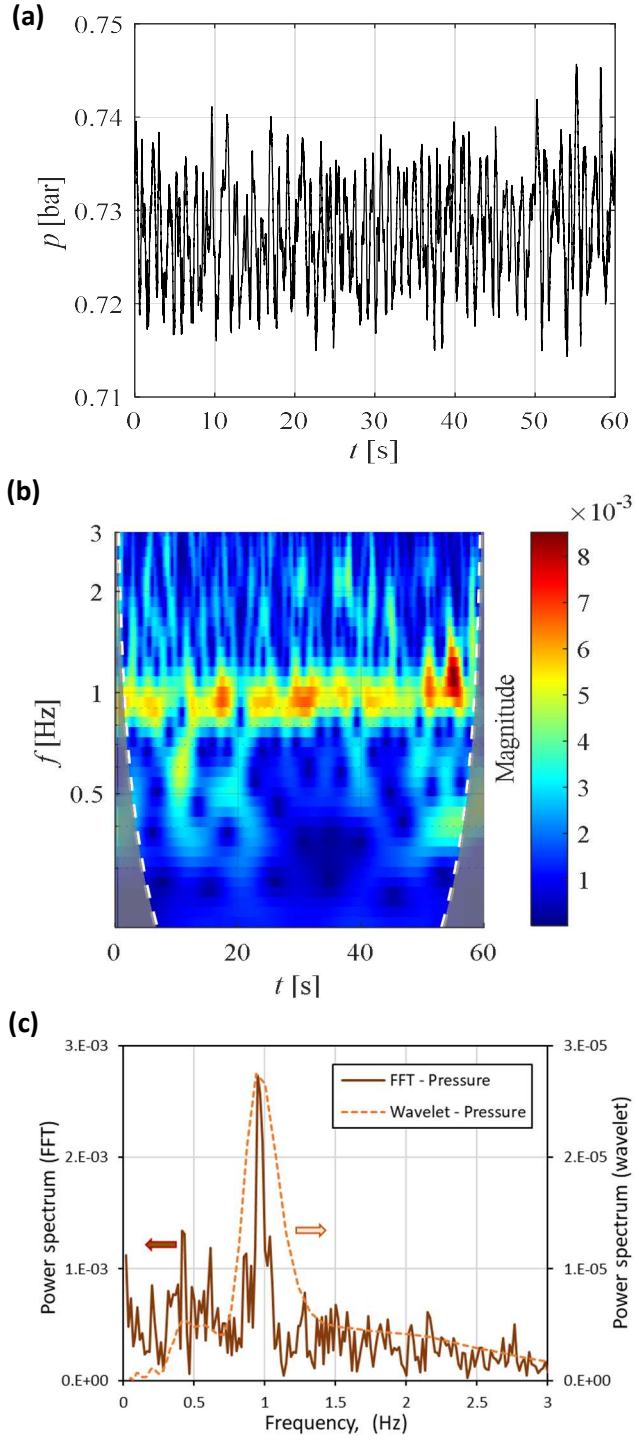

Fig. 7 (a) Raw pressure signal corresponding to Fig. 6; (b) wavelet magnitude scalogram; (c) power spectra for both FFT and wavelet methods (α = 90°; $\dot{Q}$ = 50 W).

The fluid pressure signal is similarly processed for the same working condition of Fig. 6. In Fig. 7, the collected fluid pressure is shown together with the FFT and wavelet method outputs. Alike the

wall temperature, the pressure signal (Fig. 7a) exhibits significant fluctuations during the PHP operation, confirming the link between fluid pressure and outer wall temperature. The dominant fluid oscillation frequency is assessed, through the FFT method, equal to 0.95 Hz (Fig. 7c). The non-fixed feature of fluid oscillations is again perceived in the magnitude scalogram of Fig. 7b, while the power spectrum outputted by the wavelet method presents a peak at 0.94 Hz. Although a very slight discrepancy between dominant oscillation frequency estimated through the FFT method and the wavelet method is here perceivable, the two values are reasonably comparable in terms of uncertainty of the approaches, which is affected by the time discretization of the raw samples.

In conclusion, the presented analysis has highlighted that the wavelet and FFT methods provide similar outcomes regardless the considered pieces of data. This evidence suggests that, contrarily to what was highlighted by Perna et al. (2019), both reduction approaches can be effectively adopted for the study of fluid oscillation frequencies in PHPs, at least when IR or fluid pressure measurements are considered. Moreover, the agreement in terms of wavelet method between frequency analysis on thermographic acquisitions and fluid pressure signals suggests that both experimental data reflect the PHP oscillatory behavior, in accordance with Pagliarini et al. (2021). Finally, achieving a robust quantification of dominant frequencies by adopting different experimental signals and reduction methods suggests that the intrinsic chaoticity of the system may not always hamper the identification of dominant frequency patterns. Specifically, the suitability of single-point pressure signals for the dominant fluid oscillation frequency evaluation in the present device agrees with the findings of Khandekar et al. (2009) for a single-loop PHP case, while it disagrees with the ones provided by Mameli et al. (2014) and Takawale et al. (2019) for multi-turn PHPs. This might be due to different reasons, including different layout or different working fluid considered in the present work, which may lead to a less chaotic oscillatory operation. In addition, at the light of the frequency analyzes carried out on IR data in previous works (Pagliarini et al., 2021,2022,2023b, Iwata et al., 2022) and in the present investigation, thermography seems to be confirmed, for different PHP configurations, as a

robust tool for evaluating dominant fluid oscillation frequencies, contrarily to what assessed in studies dealing with thermocouples signals, where the data reduction sometimes failed to catch the fluid oscillatory behavior (Zhao et al., 2011; Monroe et al., 2018). Further studies on the best signals and reduction techniques to be used for frequency investigations in PHPs must be therefore conducted with the aim of fully proving the feasibility of different approaches on varying PHP layouts and collected experimental data.

(ii) ***FFT analysis: influence of orientation and heat power applied***

Once established that the post-processing procedure does not affect, at least for the present investigation case, the goodness of the final results, the FFT method has been chosen for a systematic quantification of dominant fluid oscillation frequencies at different operating conditions of the studied device. Both IR (10 Hz, 120 s) and fluid pressure data (100 Hz, 160 s) were taken into account during nearly steady-state conditions for every heat power step and orientation –except the nonfunctional horizontal orientation-. Specifically, the fluid pressure signals were filtered by means of a one-dimensional Gaussian kernel to reduce possible unwanted noise from the raw data. This pre-processing is regarded to allow better outcomes, improving the readability of power spectra in terms of dominant frequencies identification.

Fig. 8 presents the dimensionless power spectra, allowing to plot all curves in the same graphs ($P_w/P_{w,max}$, $P_{w,max}$ being the maximum power spectrum over the frequency range of each series), resulting from the FFT of pressure signals for the four inclination angles (from 22.5° to 90°), and four heat powers applied (25 W and 50 W for Fig. 8a, and 100 W and 150 W for Fig. 8b). Note that the absolute power spectra can be seen in Appendix. On the one hand, in the case of Fig. 8a for the lowest heat loads, the frequency peak is particularly pronounced and almost equal for the four inclinations at 25 W, but it shows a slight divergence for the 22.5° inclination at 50 W. On the other hand, in the case of higher heat loads of Fig. 8b, the frequency peaks tend to spread and diverge from each other at 100 W, particularly for the 22.5° inclination. At heat loads greater or equal to 150 W, peaks in the power

spectra seem to fade away, and are instead observed around 0.5 Hz, which also exists for the other heat power levels. Such a drop in dominant fluid oscillation frequency at high heat loads to the evaporator (from 150 to 200 W) reflects the slight increase in thermal resistance assessed in Section 3.1 for all the orientations. In fact, weaker fluid oscillations may lead to poorer heat transfer capabilities of the device, eventually undermining the overall device operation.

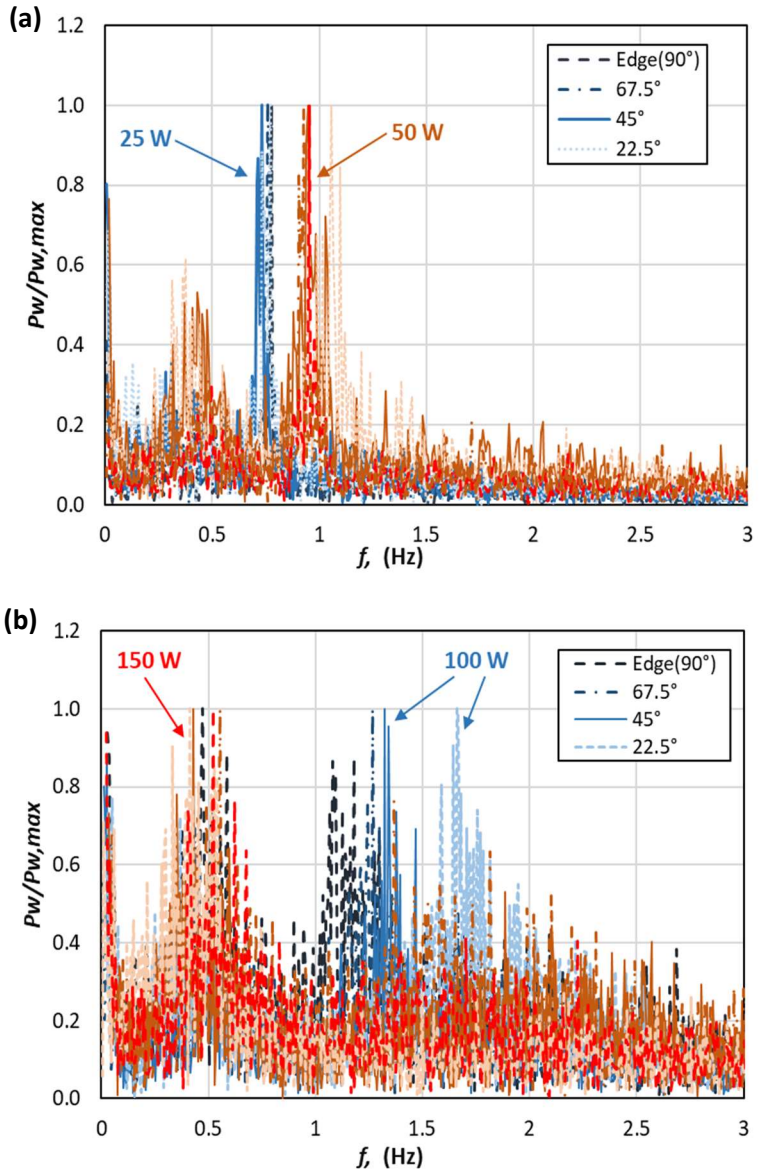

Fig. 8 Dimensionless power spectra from FFT analysis of pressure signals for different inclination angles: (a) $\dot{Q} = 25$ W (blue curves) and 50 W (brown-red curves); (b) $\dot{Q} = 100$ W (blue curves) and 150 W (brown-red curves).

Fig. 9 presents a set of FFT power spectra functions of frequency for the eight averaged IR signals windows recorded in edge inclination at 50 W heat power applied. It can be observed that, as mentioned on Fig. 6 and 7, the dominant temperature oscillation frequencies peaks are also very pronounced, and are the same for all the U-turns, as well as for the pressure signal (0.95 Hz). Therefore, the oscillations observed for both pressure and resulting temperatures at the outside wall of the FPPHP fit well together, the first being the direct cause of the second. There is indeed a transmission of the liquid plugs flow by the spring effect of the vapor bubbles from one turn to another, leading to such detectable periodic behavior of the temperature signals outside the channels wall, as already observed in (Miyazaki and Arikawa, 1999; Kim et al., 2003; Ayel et al., 2014; Pagnoni et al., 2018). Only note that no clear oscillation dominant frequency was found for U-turns 3 and 6 in the case of Fig. 9.

Furthermore, the number of IR windows for which no dominant frequencies are detected increases with increasing heat loads, and the dominant frequencies are also more hardly detectable for IR thermographs signals at 100 W heat power than for pressure signal. This can be explained by two phenomena: first, when the inner fluid dynamics becomes more chaotic due to a complex interplay between phase-change phenomena, buoyancy forces and capillary effects of the rectangular grooves, outer wall temperature data may not be able to fully catch the oscillatory behavior of the system; secondly, the thermal inertia of the evaporator wall could also attenuate the increasing frequency of transient inner surface temperature (low-pass filter). Such limitations of IR thermography in terms of inner fluid dynamics assessment were also observed in (Pagliarini et al., 2023c), where fluid velocities could not be always estimated starting from outer wall temperature signals due to the high chaoticity of the fluid stream at high heat loads (i.e., where inertial forces became more predominant).

Anyway, increasing heat power also implies the vanishing of some dominant frequencies of the pressure signal, leading to some more chaotic flow. It seems that, for low heat flux, the fluid flow is rather governed by gravity forces, triggered by pressure disturbances caused by temperature differences between channels, leading to some periodic oscillating flow as it was observed for heat

409 powers lower than 100 W, whereas the irregular pressure perturbations governed by high heat flux
410 become preponderant above a certain value, although assisted by the gravity pressure head, and leading
411 to some non-periodic oscillating-chaotic flow. Boundary between both –periodic and chaotic- regimes
412 is rather blurry, surely depending on operating conditions (working fluid, filling ratio, dimensions,
413 temperature, etc.). This point should also be further clarified.
414

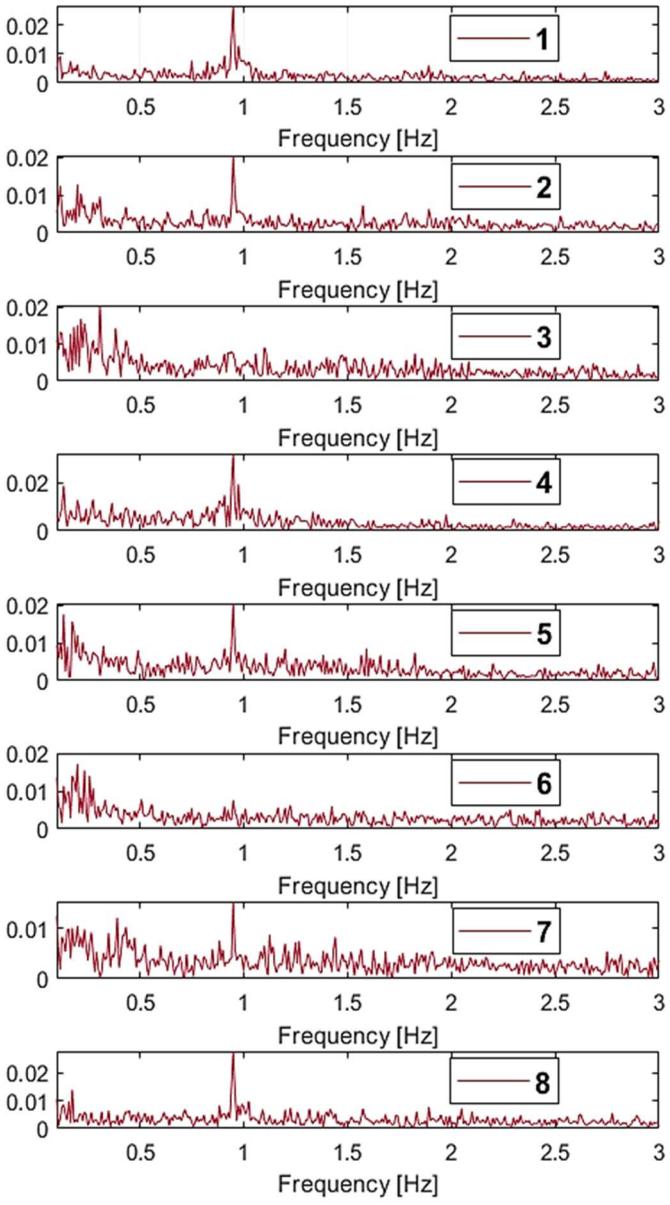

415

416 **Fig. 9** Power spectra from FFT analysis of IR thermographic signals (α = 90°; $\dot{Q}$ = 50 W).

417

Finally, all the dominant frequencies obtained by FFT analyzes for both pressure (lines) and IR thermographs (markers) signals are plotted in Fig. 10, together with the uncertainty bars resulted from the observation of the frequency ranges in which peaks in the power spectra were scattered (such ranges increased in width with the increase of the heat load, as highlighted in Fig. 9). This graph, however, hides the fact that several points from the IR thermographs are nearly perfectly superimposed due to the regularity of the oscillations, as already seen in Fig. 9. Whatever, values obtained for both signals are very close, those of the IR thermographs being always included in the error bars of the pressure signals.

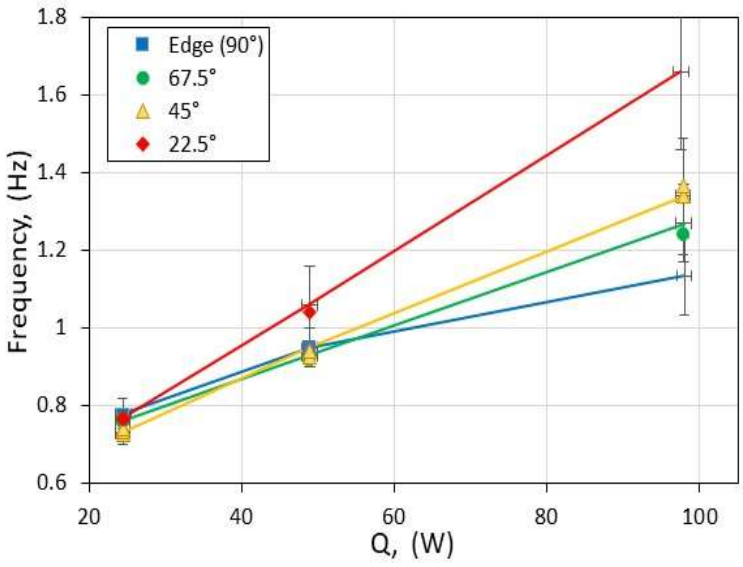

Fig. 10 Dominant frequencies of IR thermographic (markers) and pressure (lines) signals as functions of heat power applied for the four orientations (α = 22.5°:90°).

Fig. 10 confirms that the oscillation frequency peaks increase with increasing heat powers applied and, at a lower level, with decreasing inclination angle, in accordance with (Borgmeyer and Ma, 2007; Zhang and Faghri, 2008; Yasuda et al., 2022). It can be seen that the dominant frequencies differ from each other above 50 W, and they seem to follow an increasing trend with decreasing inclination angle (corresponding to a decreasing gravity pressure head). The curve corresponding to

436 an inclination angle of 22.5° (red line and markers) is clearly detached from the others, above 25 W
437 heat power applied. Lastly, for heat loads lower than 50 W, all dominant frequencies converge towards
438 the same value, showing the regularity of the periodic flow regardless of heat flux at the evaporator.
439 From Fig. 4 and 10, it appears that the edge position is really interesting in that it allows efficient heat
440 transfer even for very low heat flux, with great regularity.

441 **4 Conclusions**

442 In this study, experimental tests were made on a flat plate pulsating heat pipe (FPPHP), filled with
443 SF33 with a filling ratio of 50%. The work aimed, on one hand, to study the suitability of different
444 experimental signals and reduction methods for the assessment of dominant fluid oscillation
445 frequencies. On the other hand, the work proposed to investigate the influence of the inclination angle
446 –from "edge" to horizontal position- and heat power applied on its thermal performances. It was found
447 that the equivalent thermal resistance increased with the increase of the tilt angle from horizontal to
448 edge positions, but it also increased with the increase of heat power above 100 W.

449 A systematic frequency analysis has been performed, using both classical FFT and Wavelet
450 methods, in order to identify the dominant frequencies of heat and fluid flows inside the device, as
451 functions of the operating conditions: inclination angles and heat power applied. The main findings
452 are summarized as follows:

453 • A comparative study between the two methods showed that both wavelet and FFT analyzes
454 provide similar results in terms of dominant frequencies.
455 • The identified dominant frequencies seem independent on the analyzed experimental signal: the
456 agreement between infrared and pressure signals indicates that, at these low levels of frequencies,
457 the fluid flow motions inside the channels of the FPPHP are phased with the resulting thermal
458 response of the wall temperature, even on the external side of the device.
459 • The suitability of both signals for estimating the dominant fluid oscillation frequency appears as
460 an opportunity to use either one or the other, depending on instrumentation possibilities.

- The FFT analysis showed that the dominant frequency of the oscillating flow increases with both increasing heat power applied and decreasing inclination angle, from edge (α = 90°) down to horizontal (α = 0°) positions, from a minimum of 0.7 Hz at low heat loads (α = 45°) to a maximum of about 1.7 Hz at high heat loads (α = 22.5°). For heat powers applied below 50 W and inclination angles higher than 45°, the dominant frequencies appear to be independent on the inclination angle.
- Finally, for highest heat power levels and whatever the inclination angle, the dominant frequency tends to fade away: the recorded spectrum becomes closer to white noise spectrum, more typical of classical PHP observations during operation.

Appendix

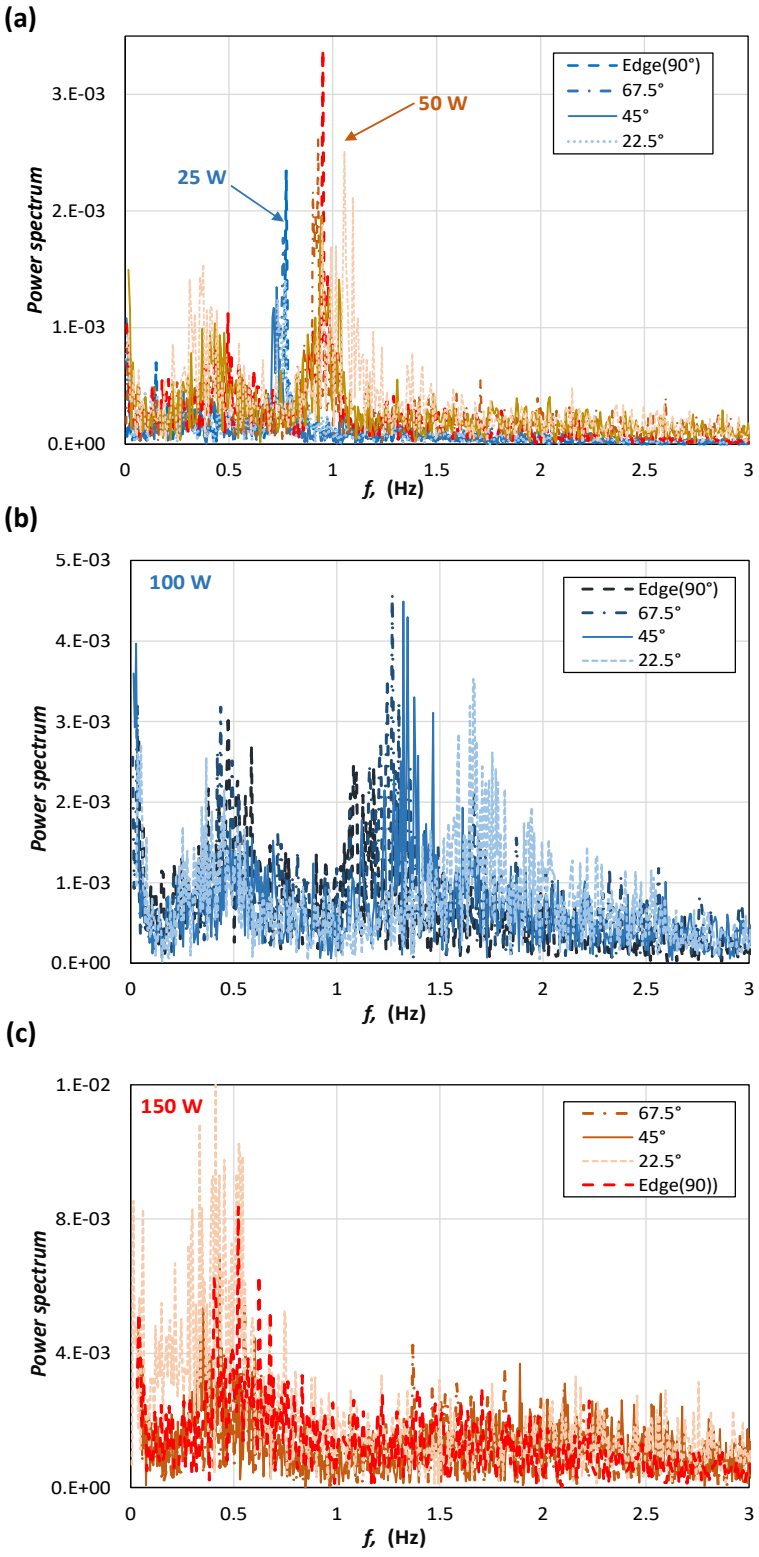

Fig. A.1 Absolute power spectra from FFT analysis of pressure signals for different inclination angles: (a) $\dot{Q} =$ 25 W (blue curves) and 50 W (brown-red curves); (b) $\dot{Q} =$ 100 W and (c) $\dot{Q} =$ 150 W.

Acknowledgements

This work has been pursued in the framework of the "Two-phase passive thermal devices for deployable space systems (TOPDESS)" project, financed through the Microgravity Application Program (N. 4000128640) by the European Space Agency. Part of this work was also carried out by CIFRE convention (ANRT program) established between Pprime Institute (Poitiers) and Stellantis (Site de Carrières-sous-Poissy) with the OpenLab Fluidics.

Declaration of competing interest

The authors have no competing interests to declare that are relevant to the content of this article.

References

Ayel, A., Romestant, C., Bertin, Y., Manno, V., Filippeschi, S. 2014. Visualization of flow patterns in flat plate Pulsating Heat Pipe: influence of hydraulic behavior on thermal performances. *Heat Pipe Science and Technology*, 5: 377-384.

Ayel, V., Slobodeniuk, M., Bertossi, R., Romestant, C., Bertin, Y. 2021. Flat plate pulsating heat pipes: A review on the thermohydraulic principles, thermal performances and open issues, *Applied Thermal Engineering*, 197: 1-37.

Borgmeyer, B.; Ma, H.B. 2007. Experimental Investigation of Oscillating Motions in a Flat Plate Pulsating Heat Pipe. *Journal of Thermophysics and Heat Transfer*. 21: 405–409

Chi, R-G., Chung, W-S., Rhi, S-H. 2018. Thermal characteristics of an oscillating heat pipe cooling system for electric vehicle Li-Ion batteries. *Energies*, 11: 1-16.

Drolen, B., Smoot, C. 2017. Performance limits of Oscillating Heat Pipes: theory and validation. *Journal of Thermophysics and Heat Transfer*, 31: 920-936.

501 Iwata, N., Bozzoli, F., Pagliarini, L., Cattani, L., Vocale, P., Malavasi, M., Rainieri, S. 2022.
502 Characterization of thermal behavior of a micro pulsating heat pipe by local heat transfer
503 investigation. *International Journal of heat and Mass Transfer*, 196: 123203.
504 Karthikeyan, V.K., Ramachandran, K., Pillai, B.C., Brusly Solomon, A. 2015. Understanding thermo-
505 fluidic characteristics of a glass tube closed loop pulsating heat pipe: flow patterns and fluid
506 oscillations. *Heat and Mass Transfer*, 51: 1669–1680.
507 Khandekar, S., Prasad Gautam, A., Sharma, P.K. 2009. Multiple quasi-steady states in a closed loop
508 pulsating heat pipe. *International Journal of Thermal Sciences*, 48: 535-546.
509 Khandekar, S., Panighahi, P-K., Lefèvre, F., Bonjour, J. 2010. Local hydrodynamic of flow in a
510 Pulsating Heat Pipe: a review. *Frontiers in Heat Pipes*, 1: 1-20.
511 Kim, J.-S., Bui, N.-H., Kim, J.-W., Jung, H. 2003. Flow visualization of oscillation characteristics of
512 liquid and vapor flow in the oscillating capillary tube heat pipe. *KSME International Journal*, 17:
513 p. 1507-1519.
514 Ma, H. 2015. *Oscillating heat pipes*, New York: Springer-Verlag Berlin Heidelberg, 427 p.
515 Mameli, M., Marengo, M., Khandekar, S. 2014. Local heat transfer measurement and thermo-fluid
516 characterization of a pulsating heat pipe. *International Journal of Thermal Sciences*, 75: 140-152.
517 Marengo, M., Nikolayev, V. 2018. Pulsating Heat Pipes: Experimental Analysis, Design and
518 Applications. In: *Encyclopedia of Two-Phase Heat Transfer and Flow IV*. Thome, J.R., Ed., Vol.
519 1: Modeling of Two-Phase Flows and Heat Transfer, World Scientific, 1-62.
520 Miyazaki, Y., Arikawa, M. 1999. M., Oscillatory flow in the Oscillating Heat Pipe. In: Proceedings of
521 the 11th International Heat Pipe Conference, 367-372.
522 Monroe, J., Aspin, Z., Fairley, J., Thompson, S. 2017. Analysis and comparison of internal and external
523 temperature measurements of a tubular oscillating heat pipe. *Experimental Thermal and Fluid*
524 *Science*, 84: 165-178.

525 Pagliarini, L., Cattani, L., Bozzoli, F., Mameli, M., Filippeschi, S., Rainieri, S., Marengo, M. 2021.
526 Thermal characterization of a multi-turn pulsating heat pipe in microgravity conditions: Statistical
527 approach to the local wall-to-fluid heat flux. *International Journal of heat and Mass Transfer*,
528 169: 120930.
529 Pagliarini, L., Cattani, L., Slobodeniuk, M., Ayel, V., Romestant, C., Bozzoli, F., Rainieri, S. 2022.
530 Novel Infrared Approach for the Evaluation of Thermofluidic Interactions in a Metallic Flat-Plate
531 Pulsating Heat Pipe. *Applied Sciences*, 12: 11682.
532 Pagliarini, L., Cattani, L., Ayel, V., Slobodeniuk, M., Romestant, C., Bozzoli, F. 2023a.
533 Thermographic investigation on fluid oscillations and transverse interactions in a fully metallic
534 Flat Plate Pulsating Heat Pipe. *Applied Sciences*, 13: 6351.
535 Pagliarini, L., Iwata, N., Bozzoli, F. 2023b. Pulsating heat pipes: Critical review on different
536 experimental techniques. *Experimental Thermal and Fluid Science*. 148: 110980.
537 Pagliarini, L., Cattani, L., Mameli, M., Filippeschi, Bozzoli, F. 2023c. Heat transfer delay method for
538 the fluid velocity evaluation in a multi-turn pulsating heat pipe. *International Journal of*
539 *Thermofluids*, 17: 100278.
540 Pagnoni, F., Ayel, V., Scoletta, E., Bertin, Y. 2018. Effects of the hydrostatic pressure gradient no
541 thermohydraulic behavior of flat plate Pulsating Heat Pipe: experimental and numerical analyses.
542 In: Proceedings of the 6th International Heat Transfer Conference, 8 p.
543 Perna, R., Abela, M., Mameli, M., Mariotti, A., Pietrasanta, L., Marengo, M., Filippeschi, S. 2020.
544 Flow characterization of a pulsating heat pipe through the wavelet analysis of pressure signals.
545 *Applied Thermal Engineering*, 171: 115128.
546 Takawale, A., Abraham, S., Sielaff, S., Mahapatra, P.S., Pattamatta, A., Stephan, P. 2019. A
547 comparative study of flow regimes and thermal performances between flat plate pulsating heat
548 pipe and capillary tube pulsating heat pipe. *Applied Thermal Engineering*, 149: 613-624.

549 Xu, J.L., Zhang, X.M. 2005. Start-up and steady thermal oscillation of a pulsating heat pipe. *Heat and*
550 *Mass Transfer*, 41: 685–694.
551 Yasuda, Y.; Nabeshima, F.; Horiuchi, K.; Nagai, H. 2022. Visualization of the working fluid in a flat-
552 plate pulsating heat pipe by neutron radiography. *International Journal of heat and Mass*
553 *Transfer*. 185: 122336.
554 Zhang, Y., Faghri, A. 2008. Advances and unsolved issues in pulsating heat pipes. *Heat Transfer*
555 *Engineering*. 29: 20–44.
556 Zhao, N, Ma, H, Pan, X. 2011. Wavelet Analysis of Oscillating Motions in an Oscillating Heat Pipe.
557 In: Proceedings of the ASME 2011 International Mechanical Engineering Congress and
558 Exposition. Volume 10: Heat and Mass Transport Processes, Parts A and B. Denver, Colorado,
559 USA, 545-549.

560

561

562 **Graphical abstract**
563

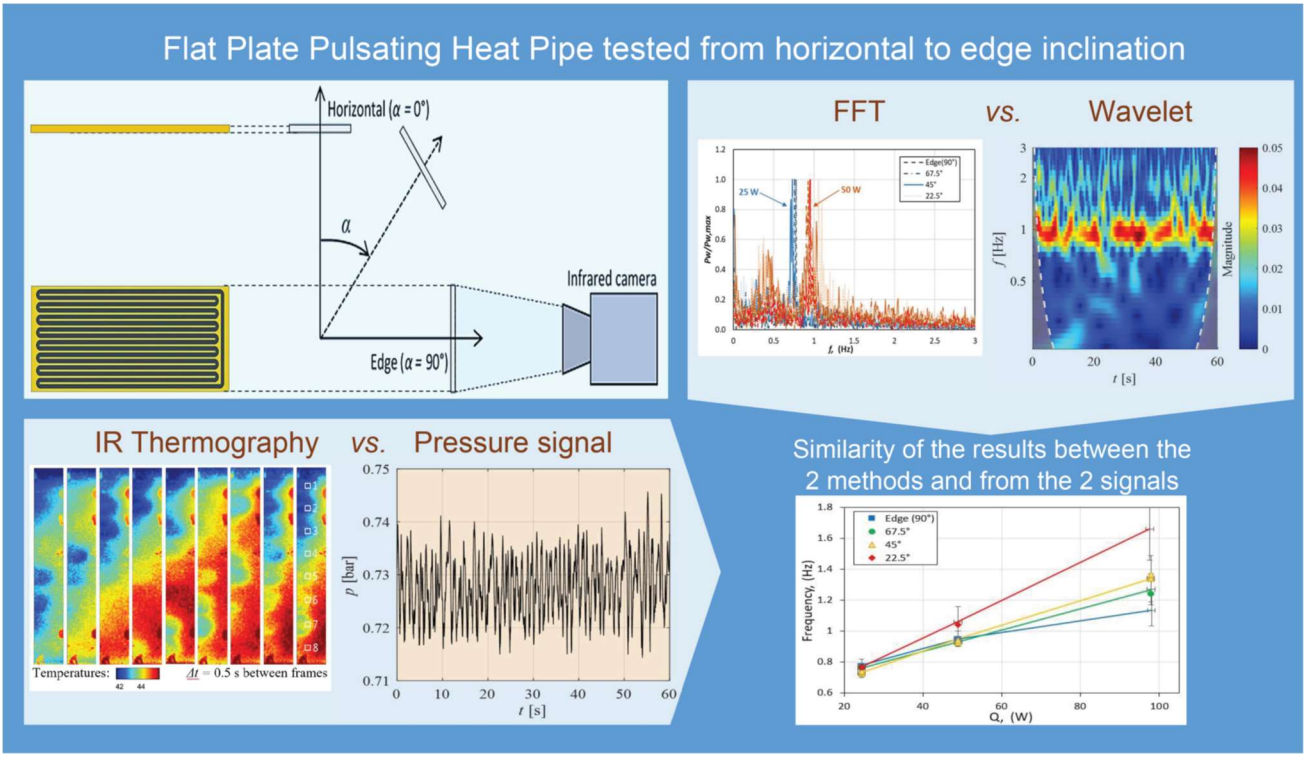

564